



VIBRATIONAL POWER FLOW IN THE MOVING BELT PASSING THROUGH A TENSIONER

Y. I. KWON[†] AND J.-G. IH

*Center for Noise and Vibration Control, Department of Mechanical Engineering, Korea
Advanced Institute of Science and Technology, Science Town, Taejon 305-701, Korea*

(Received 2 June 1998, and in final form 17 June 1999)

Because of the high performance and low weight requirements for modern machines including engines, the belts servicing high dynamic loads at high speed tend to be very susceptible to the transferred vibration. In this paper, a method is proposed for obtaining the physical characteristics of the transverse vibrational power flow through moving rubber belts. The governing equation is derived by applying Hamilton's principle to the description of the flexural vibrations in axially moving belts, where the tensioner is considered to be a one-degree-of-freedom system. The total power flow calculated and measured in the moving belt is the sum of the true power flow and the power component associated with the steady medium motion. Consequently, any component that is due solely to the belt movement should be subtracted from the total power flow in order to obtain the true, net power flow. This concept is employed in calculating the transverse vibrational power flow through belt-pulley systems that include a tensioner. An equivalent system including an idler instead of the tensioner is also considered, and the observed power flow in this condition is ascribed to the power flow due only to the movement of the medium. The results of analysis show that the vibrational power of the two belt-spans flows into the tensioner. It is shown that the energy flow, measured by using two laser sensors, agrees reasonably well with the predicted results.

© 2000 Academic Press

1. INTRODUCTION

Although belts are commonly used in various mechanical systems, many problems such as belt span resonance and fluctuation often result from high dynamic loads and high moving velocity of the belt [1]. Vibration problems in moving belts have been handled by analytical models dealing with belt spans [2–5]. It was found that the response of belts near resonance under high running speeds is dominated by the non-linear effect. Moon and Wickert [6] studied analytical and experimental models considering the non-linear effect. In order to identify the resonance condition, they used the frequency diagram of the belt relating the linear natural frequencies and the speed-dependent excitation frequencies originating from

[†] Currently working at the Noise and Structure Research Team, Central Research Center, Hyundai Motor Co., Kusung-myon, Yongin-si, Kyungki-do 449-910, Korea.

pulleys having eccentricities. The vibration of belts considering the coupling between spans with pulleys has also been of concern [7–12].

Although the vibration power of belt span itself has been generally of interest, this paper introduces the analytical and experimental methods to obtain the vibrational power transmission from the moving belt into the support system. This consideration is because the traditional heavy materials of pulley and supporting structure have been replaced by lightweight plastics and aluminum and these materials are weak in vibration and easily excited by the belt. In order to reduce the vibration level of each belt span, idler and/or tensioner mechanisms are now added in between the drive and the driven pulleys [13]. These additions easily transfer vibrational power from one source to many parts, especially when many components are connected and driven by a single belt. Consequently, solutions to noise and vibration problems can be sought for in the light of reducing the vibrational power transmission through pulleys and the tensioner connected to the moving belt.

The time-averaged input power flow into the idler and tensioner from the moving belt can be written as

$$\langle \dot{H} \rangle_I = m|V|^2\omega/2, \quad (1)$$

where m is the mass and V is the transverse velocity of idler or tensioner. The vibrational powers of idler and tensioner were measured by using a laser sensor and the results are shown in Figure 1. The vibration of the idler and the tensioner was caused by the transverse vibration of the belt span. One can find that the vibration power level in the idler condition is much lower than that in the tensioner condition. Major peaks of the vibrational power spectrum of the tensioner consist of three components: first, power transmitted from the connected belt spans; second, rotating frequency of the tensioner and their harmonics; third, direct excitation from the belt discontinuity. The vibration power of the bearing and the structure supporting this tensioner causes the vibration and noise problems. A reduction in vibrational power and subsequently acoustical radiation may be attained by controlling the net vibrational power flow through the belt. Analytical methods were introduced for correctly calculating the energy and power flow in the axially moving media [14, 15].

In this paper, a method is proposed for investigating the characteristics of the transverse vibrational power flow through the moving rubber belt. The structural intensity method used has been applied to stationary uniform [16] or multi-supported beams [17, 18]. The total power flow in the moving medium is the sum of the components associated with the true power flow and the movement of medium itself. The latter, due to the difference between wave numbers in opposite directions, will not carry actual power flow. Consequently, any component associated with the moving medium should be subtracted from the total power flow in order to obtain the true power flow. By utilizing the beam model without damping the total power can be dissolved into the true power and the component associated with the moving medium only. This concept is employed in the calculation of transverse vibrational power flow through belt–pulley systems that include a tensioner.

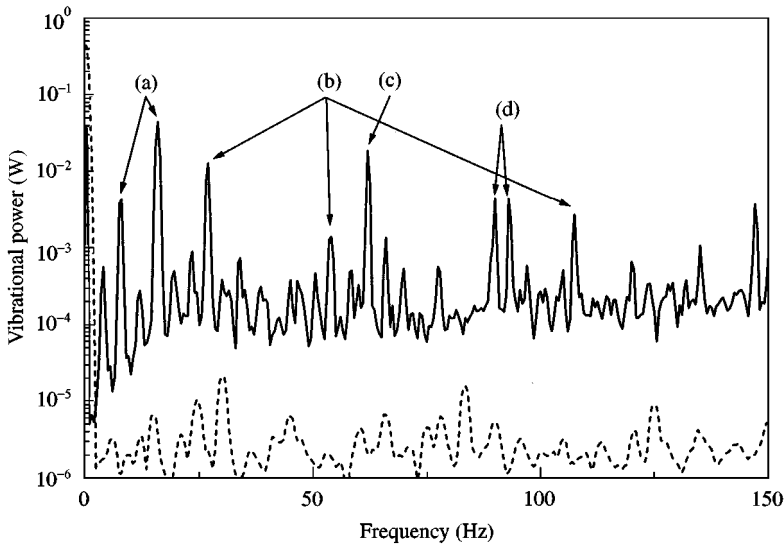


Figure 1. Measured spectra of the vibrational power of idler and tensioner -----, idler; ———, tensioner. Peaks are related to (a) direct input power from the belt discontinuity, (b) rotating frequency of the tensioner and their harmonics, (c) vibration component caused by the power flow from the second span, (d) vibration components caused by the power flow from the first span.

2. THEORY

As shown in Figure 2, a tensioner is located between the drive and the driven pulleys. Usually, longitudinal, torsional, and transverse vibrations of the belt are coupled. Since only the transverse vibrational power flow is addressed in this paper, it will focus on how the vertical motion of the tensioner is affected by the transverse vibration of the rubber belt. Although the system has three spans, l_1 , l_2 , l_3 , only the transverse vibration transmission between the first and second spans, l_1 , l_2 , will be considered in this paper.

Excitation of transverse vibration is in general caused by the interactions of belt and pulleys such as the non-circularity or eccentricity of the pulley system, the surface irregularity of belt and pulley, and the dynamic loading [3, 19, 20]. Imperfections in belt stiffness such as the end connection of the belt [21] excite the belt in the transverse direction. This paper will show that the dynamic properties of the belt tensioner function significantly in changing the characteristics of the vibrational power transmission.

2.1. BASIC GOVERNING EQUATION

The equation of motion for the small-amplitude transverse vibration of the axially moving belt has generally been derived through Hamilton's principle. The variation of time integral of the kinetic energy minus the potential energy of a section of the belt between supports is zero. In this study, since the wavelength of the transverse vibration of interest is much longer than the thickness of the belt,

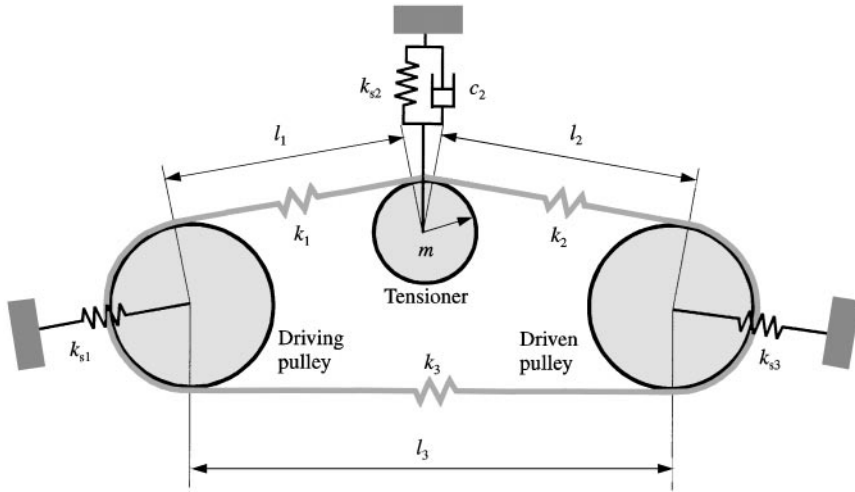


Figure 2. Geometry of the typical belt-pulley system.

rotary inertia and shear deformation effects are ignored. From the Euler-Bernoulli beam model, the equation of motion for the belt under an initial tension R_0 can be written as [8]

$$\rho A \frac{\partial^2 w_i}{\partial t^2} + 2\rho A c \frac{\partial^2 w_i}{\partial x \partial t} + (\kappa_i \rho A c^2 - R_0) \frac{\partial^2 w_i}{\partial x^2} + EI \frac{\partial^4 w_i}{\partial x^4} = 0, \quad (2)$$

where ρ is the density of the belt, A is the cross-sectional area of the belt, E is the modulus of elasticity, I is the area moment of the belt cross-section, w_i is the transverse displacement of the i th belt span, c is the band axial velocity, $\kappa_i = 1 - \zeta_i$, and ζ_i is the pulley support constant of the i th belt span. If a general damping force is added which is proportional to the velocity as $\beta c (\partial w / \partial t) + \beta (\partial w / \partial x)$, equation (2) can be rewritten as

$$\rho A \frac{\partial^2 w}{\partial t^2} + 2\rho A c \frac{\partial^2 w}{\partial t \partial x} + (\kappa_i \rho A c^2 - R_0) \frac{\partial^2 w}{\partial x^2} + \beta c \frac{\partial w}{\partial t} + \beta \frac{\partial w}{\partial x} + EI \frac{\partial^4 w}{\partial x^4} = 0, \quad (3)$$

where β is the proportion constant. The first term in equation (3) is the centrifugal force caused by the instantaneous curvature, the second term is the Coriolis force generated by the combined linear and rotational motions, and the third term is the tension force. In general, when a belt is initially tightened around two or more pulleys, when driven by the rotation of one of them, it will transmit force by tension. The difference in the belt tensions on the entering and leaving sides of any pulley is the force transmitted to the pulley. In the two-pulley arrangement having diameters of D and D' , respectively, the force transmitted to the pulley is $R_T - R_L$ where R_T is called the tight-side tension and R_L the loose-side tension. The torques developed, T and T' , are given by

$$T = (R_T - R_L) D / 2 \quad \text{and} \quad T' = (R_T - R_L) D' / 2, \quad (4)$$

where the ratio $T'/T = D'/D$ holds. Under the loading condition, the belt tension is velocity-dependent and, at an axial transportation speed c , the tight-side tension of moving belt, \bar{R}_T , and the loose-side tension of moving belt, \bar{R}_L , can be expressed as

$$\bar{R}_T = R_T + \zeta_T \rho A c^2 = R_T + (1 - \kappa_T) \rho A c^2, \quad (5a)$$

$$\bar{R}_L = R_L + \zeta_L \rho A c^2 = R_L + (1 - \kappa_L) \rho A c^2. \quad (5b)$$

Here, ζ_T and ζ_L are pulley support constants of the tight-side and loose-side belt span, respectively, $\kappa_T = 1 - \zeta_T$, and $\kappa_L = 1 - \zeta_L$. Under idling or no-torque conditions, $R_T = R_L$ because there is no tension difference at each span. Although the tension under loading and moving belt condition can be easily expressed by using equations (5a) and (5b), only the idling or no-torque condition is investigated in this paper.

The tension of the i th belt span is related to the stationary tension as follows [2]:

$$R_i = R_0 + \zeta_i \rho A c^2 = R_0 + (1 - \kappa_i) \rho A c^2. \quad (6)$$

The pulley support constant ζ_i is defined by [22]

$$\zeta_i = \frac{k_i \delta_i}{\rho A c^2}, \quad (7)$$

where k_i is the stiffness of each belt in the axial direction and δ_i is the axial displacement of each span. In Figure 3, the spring constants of the driving and driven pulley bearings are identically 8×10^5 N/m, and the pulley support constants for the first and second spans are calculated by changing the spring constant of the tensioner. The pulley support constants of the first and second spans converge from 1 into a small value near to 0 as the spring constant of the tensioner increases. The pulley support constant of each span generally differs from each other within the practical range of the spring constant of the tensioner.

A steady state response due to the harmonic excitation for the axially moving belt is assumed as

$$w_i(x, t) = W_i(x) \exp(j\omega t), \quad (8)$$

where $j = \sqrt{-1}$. By substituting equation (8) into equation (3), one can obtain

$$\begin{aligned} -\rho A W_i(x) \omega^2 + 2j\rho A c \frac{\partial W_i(x)}{\partial x} \omega + (\kappa_i \rho A c^2 - R_0) \frac{\partial^2 W_i(x)}{\partial x^2} \\ + \beta W_i(x) + \beta c \frac{\partial W_i(x)}{\partial x} + EI \frac{\partial^4 W_i(x)}{\partial x^4} = 0. \end{aligned} \quad (9)$$

By introducing $W_i(x) = \exp(\lambda_i x)$, one can rewrite equation (9) as

$$EI\lambda^4 + (\kappa\rho A c^2 - R)\lambda^2 + (\beta c + 2\rho A c\omega)\lambda + j\beta\omega - \rho A\omega^2 = 0. \quad (10)$$

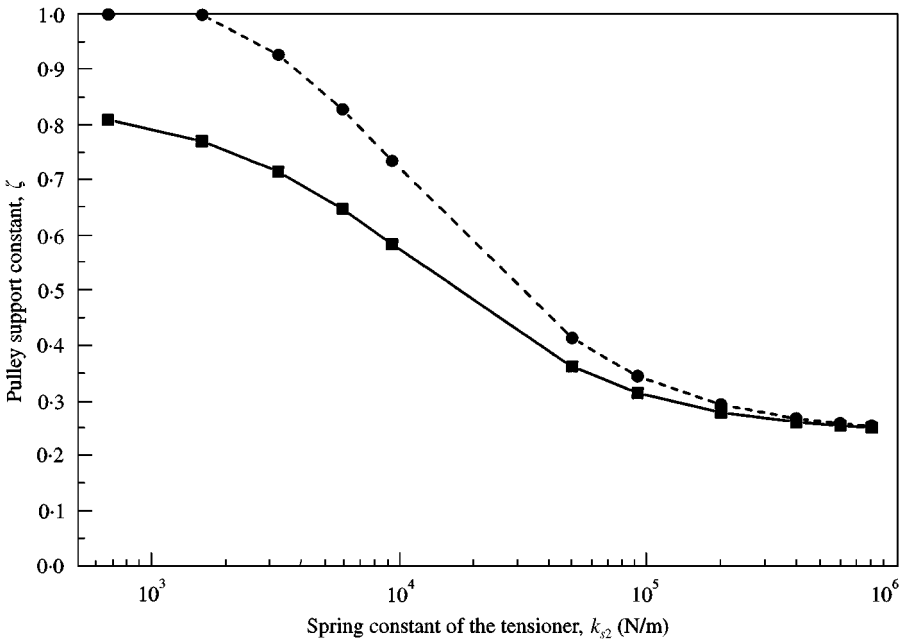


Figure 3. Pulley support constant as a function of the spring constant of the tensioner: -●-, first span; —■—, second span.

In contrast to the undamped and stationary belt, the damped and moving belt will have complex roots. The four roots of equation (10), $\lambda_1, \lambda_2, \lambda_3, \lambda_4$, can be obtained numerically. Then, the general solution $W_i(x)$ will be

$$W_i(x) = A_i \exp(\lambda_1 x) + B_i \exp(\lambda_2 x) + C_i \exp(\lambda_3 x) + D_i \exp(\lambda_4 x). \tag{11}$$

The unknown coefficients A_i, B_i, C_i, D_i can be determined from the given boundary conditions and the following matrix equation can be formed:

$$[Z(\omega)]\{W\} = \{F\}. \tag{12}$$

Here, $[Z(\omega)]$ is called the impedance matrix for axially moving belt, $\{W\}$ contains unknown coefficients and $\{F\}$ represents the excitation amplitude. Provided that $[Z(\omega)]^{-1}$ exists, the unknown coefficients A_i, B_i, C_i, D_i can be obtained by numerically solving the following equation:

$$\{W\} = [Z(\omega)]^{-1}\{F\}. \tag{13}$$

Then, equation (8) as the solution of equation (3) can be written as

$$w_i(x) = (A_i \exp(\lambda_1 x) + B_i \exp(\lambda_2 x) + C_i \exp(\lambda_3 x) + D_i \exp(\lambda_4 x)) \exp(j\omega t). \tag{14}$$

Consider the transverse vibration of the axially moving belt span as shown in Figure 4. The boundary conditions of this model are given by

$$w(0, t) = w_0 \exp(jq\omega_p t), \quad \left. \frac{\partial^2 w}{\partial x^2} \right|_{x=0} = 0, \quad \left. \frac{\partial^2 w}{\partial x^2} \right|_{x=l} = 0, \quad w(l, t) = 0, \tag{15-18}$$

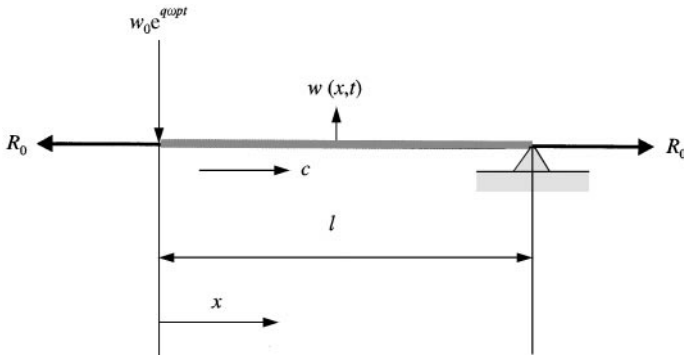


Figure 4. Schematic diagram of the belt span modelled as an axially moving beam.

where q denotes the number of excitation events at the end $x = 0$ and the system is simply supported at $x = l$. Substituting the solution into equations (15)–(18), the frequency response function $[Z(\omega)]^{-1}$ can be obtained and it is a function of belt speed. The variation of frequency response function with the belt speed is shown in Figure 5, which reveals the fact that the first natural frequency of moving belt decreases as the belt speed increases. Figure 6 shows that the natural frequency of the belt decreases as the belt thickness increases and also the same frequency shift as in Figure 5 can be seen.

2.2. POWER FLOW IN THE MOVING BELT

The flexural wave causes two internal forces to act in the belt: one associated with bending and the other associated with moment. Both these forces are important in carrying the vibrational power. The total vibrational power flow along the belt considering the aforementioned two components is given by [16]

$$\langle \Pi \rangle_T = \frac{EI}{2} \operatorname{Re} \left\{ \left[\frac{\partial^3 w_i(x, t)}{\partial x^3} \right] \left[\frac{\partial w_j(x, t)}{\partial t} \right]^* - \left[\frac{\partial^2 w_j(x, t)}{\partial x^2} \right] \left[\frac{\partial^2 w_j(x, t)}{\partial x \partial t} \right]^* \right\}, \quad (19)$$

where the asterisk denotes the complex conjugate. The structural intensity formula in equation (19) has been used to calculate and measure the vibration power flow in the stationary structures. In order to apply this method to moving belts, the components carrying no vibration power should be removed from the total power flow; this is because the absolute wave numbers in opposite directions differ from each other. As wave speed, wavelength, and wave number of the downstream become higher, longer, and smaller, respectively, corresponding upstream properties become lower, shorter, and larger. These factors cause the phase delay along the belt due to the Coriolis force in equation (3). There will be no actual power flow associated with the belt movement.

True power flow in the moving belt can be analyzed by using the moving beam model without damping. Power flow due to the bending moment in the stationary beam is the same that from the shear force at a point far away from boundaries [23]. In this case, the power flow can be calculated if one of the two components is

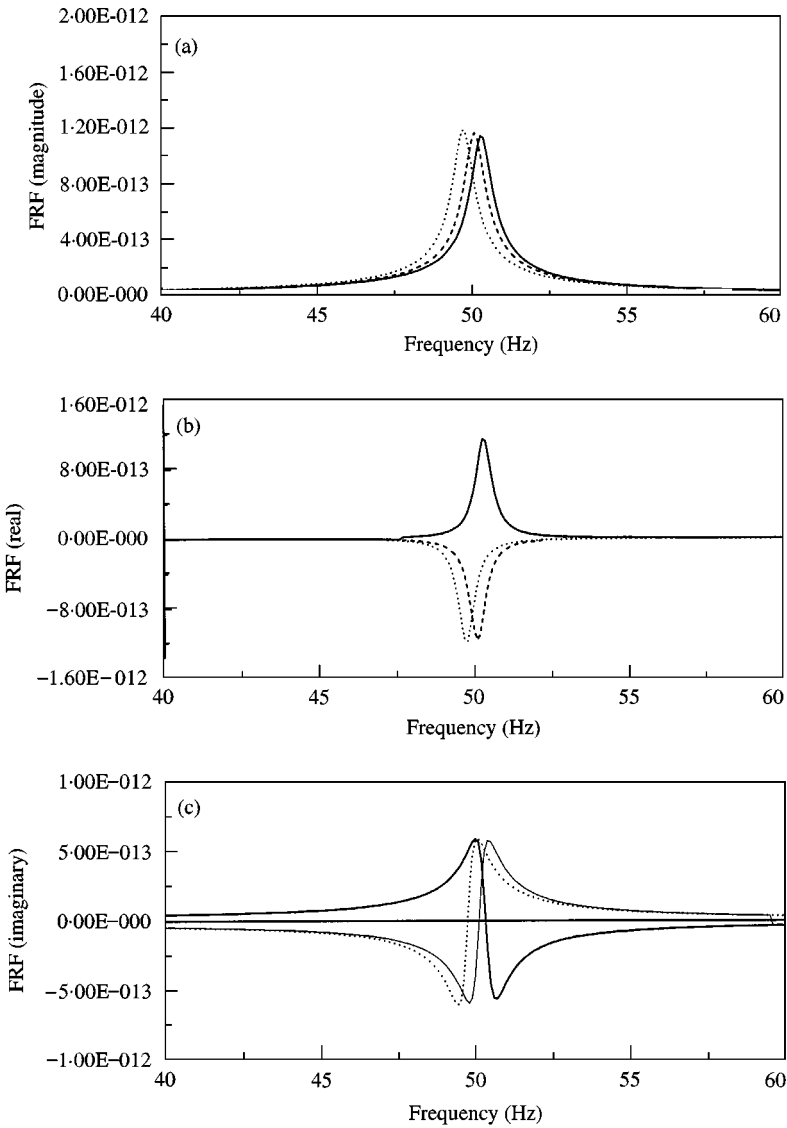


Figure 5. Magnitude, real and imaginary part of $[Z(\omega)]^{-1}$ varying the moving speed: —, 500 r.p.m.; ----, 1000 r.p.m.; ·····, 1500 r.p.m.

calculated and simply doubled. However, these two components are no longer the same when the wave numbers for two opposite directions are not the same. The moment and shear components of the power flow in the moving beam can be written as

$$\langle \Pi_M \rangle = -\frac{EI}{2} \operatorname{Re} \left\{ \left[\frac{\partial^2 w(x, t)}{\partial x^2} \right] \left[\frac{\partial^2 w(x, t)}{\partial x \partial t} \right]^* \right\}, \quad (20)$$

$$\langle \Pi_F \rangle = \frac{EI}{2} \operatorname{Re} \left\{ \left[\frac{\partial^3 w(x, t)}{\partial x^3} \right] \left[\frac{\partial w(x, t)}{\partial t} \right]^* \right\}, \quad (21)$$

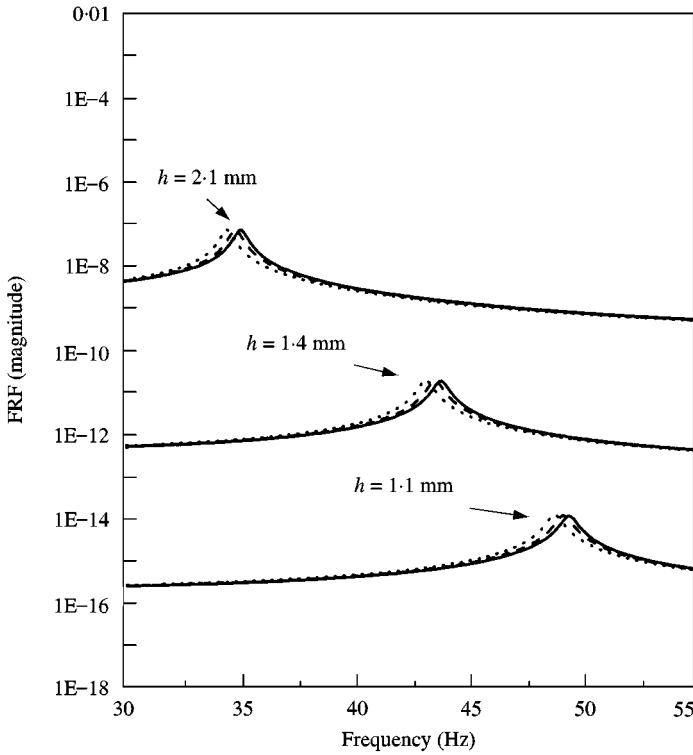


Figure 6. Variation of magnitude of $[Z(\omega)]^{-1}$ varying the thickness and the moving speed: —, 500 r.p.m.; - - - -, 1000 r.p.m.; ·····, 1500 r.p.m.

where $\langle \Pi_M \rangle$ is the time-averaged power flow associated with the moment and $\langle \Pi_F \rangle$ is that associated with the shear force. The nearfield component is negligible where it is sufficiently far from the discontinuities. When the reflection coefficient R is introduced, the transverse displacement can be expressed as

$$w(x, t) = A[\exp(-jk_{b1}x) + R \exp(jk_{b2}x)] \exp(j\omega t), \tag{22}$$

where k_{b1} , k_{b2} are the wave numbers in downstream and upstream directions respectively. By using equations (20)–(22), one can derive the following power quantities:

$$\langle \Pi_M \rangle = \frac{EI}{2} \omega |A|^2 \{ (k_{b1}^3 - |R|^2 k_{b2}^3) - |R| (k_{b1}^2 k_{b2} - k_{b1} k_{b2}^2) \cos[(k_{b1} + k_{b2} + \phi)x] \}, \tag{23}$$

$$\langle \Pi_F \rangle = \frac{EI}{2} \omega |A|^2 \{ (k_{b1}^3 - |R|^2 k_{b2}^3) + |R| (k_{b1}^3 - k_{b2}^3) \cos[(k_{b1} + k_{b2} + \phi)x] \}, \tag{24}$$

$$\begin{aligned} \langle \Pi \rangle_T = \langle \Pi_F \rangle + \langle \Pi_M \rangle &= \frac{EI}{2} \omega |A|^2 \{ 2(k_{b1}^3 - |R|^2 k_{b2}^3) \\ &+ |R| (k_{b1} - k_{b2})(k_{b1}^2 + k_{b2}^2) \cos[(k_{b1} + k_{b2} + \phi)x] \}. \end{aligned} \tag{25}$$

Here, $\langle \Pi \rangle_T$ means the total power flow and ϕ is the phase difference between upstream and downstream waves. It is noted that the power flow due to the moment is different from that due to the shear.

When all progressive waves are totally reflected at the boundary, R is 1 and equations (23) and (24) can be rewritten as

$$\langle \Pi_M \rangle = \frac{EI}{2} \omega |A|^2 \{ (k_{b1}^3 - k_{b2}^3) - (k_{b1}^2 k_{b2} - k_{b1} k_{b2}^2) \cos[(k_{b1} + k_{b2} + \phi)x] \}, \quad (26)$$

$$\langle \Pi_F \rangle = \frac{EI}{2} \omega |A|^2 \{ (k_{b1}^3 - k_{b2}^3) + (k_{b1}^3 - k_{b2}^3) \cos[(k_{b1} + k_{b2} + \phi)x] \}. \quad (27)$$

Because $k_{b1} < k_{b2}$ for a constant moving beam, the total power flow is always negative, i.e. $\langle \Pi \rangle_T < 0$. The increase in power flow with belt speed is caused by the difference in wave numbers. However, this is physically meaningless, because the negative total power implies that the reflective power becomes larger than the incident power. Consequently, it can be said that the total power includes the components carrying both the net power flow and the power flow associated with the moving medium. This can be written as

$$\langle \Pi \rangle_T = \langle \Pi_{true} \rangle + \langle \Pi_{mov} \rangle \quad \text{or} \quad \langle \Pi_{true} \rangle = \langle \Pi \rangle_T - \langle \Pi_{mov} \rangle, \quad (28a, b)$$

where $\langle \Pi_{true} \rangle$ is the component of the actual power flow and $\langle \Pi_{mov} \rangle$ is the power flow associated with the medium movement. When $\langle \Pi_{true} \rangle = 0$, $\langle \Pi \rangle_T$ equals the component associated only with the medium motion. This means that the incident power is equal to the reflective power. The component $\langle \Pi_{mov} \rangle$ can be calculated from equation (25) with $|R|^2 = 1$ as

$$\begin{aligned} \langle \Pi \rangle_T = \langle \Pi_{mov} \rangle &= \frac{EI}{2} \omega |A|^2 \{ 2(k_{b1}^3 - k_{b2}^3) \\ &+ (k_{b1}^2 + k_{b2}^2)(k_{b1} - k_{b2}) \cos[(k_{b1} + k_{b2} + \phi)x] \}. \end{aligned} \quad (29)$$

When $|R|^2 < 1$, there exists the true power flow. Using equations (25) and (28b), the true power flowing through the moving beam can be derived as

$$\begin{aligned} \langle \Pi_{true} \rangle &= \frac{EI}{2} \omega |A|^2 (1 - |R|) \{ 2(1 + |R|)k_{b2}^3 \\ &- (k_{b1}^2 + k_{b2}^2)(k_{b1} - k_{b2}) \cos[(k_{b1} + k_{b2} + \phi)x] \}. \end{aligned} \quad (30)$$

As a limiting case, when $k_{b1} = k_{b2} = k_b$ and $|R|^2 \rightarrow 0$ in equation (30), the power flow in the stationary semi-infinite beam can be calculated as $\langle \Pi_{true} \rangle = EI\omega |A|^2 k_b^3$.

2.3. CHARACTERISTICS OF THE SINGLE SPAN BELT

In order to implement equation (3), the modulus of elasticity and the damping coefficient were experimentally determined. First, the belt was excited into vibration by an impact hammer, and natural frequencies were obtained from the frequency response function. The modulus of elasticity was calculated by

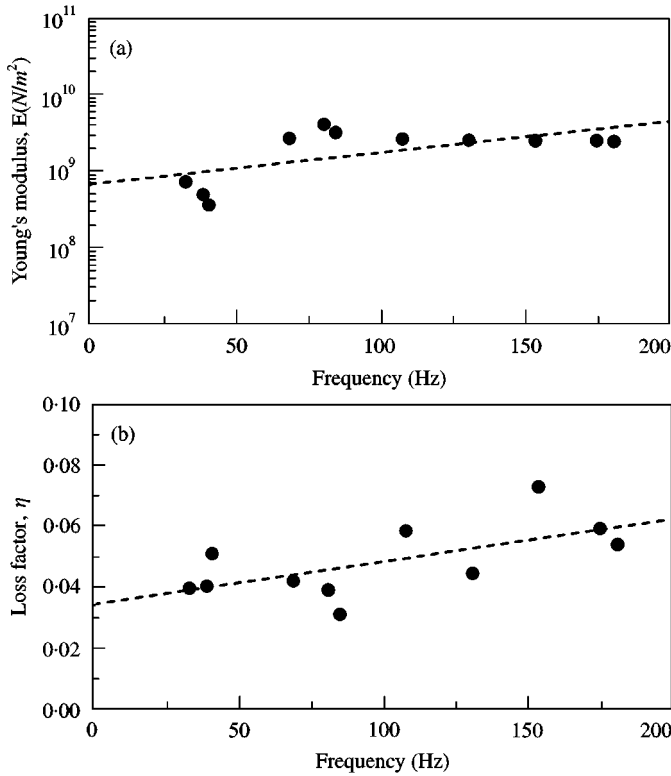


Figure 7. Measured Young's modulus and loss factor: ●, measured data; ---, linear regression.

substituting the measured natural frequencies into the tensioned beam model. As shown in Figure 7(a), a linear regression line was obtained for the evaluated modulus of elasticity data. An increasing trend with frequency can be seen: $E = (1.018f + 112.6) \times 10^7 \text{ N/m}^2$ with the standard deviation of 1.1×10^9 , where f is the frequency in Hz. Loss factor was obtained by using the half-power bandwidth method. As shown in Figure 7(b), loss factor increases with frequency as $\eta = (1.33f + 340) \times 10^{-4}$ having the standard deviation of 0.011. Linearly fitted loss factor can be converted into the damping coefficient by

$$\beta = \eta m_n \omega_n, \quad (31)$$

where ω_n are natural frequencies, $m_n = \int_0^l \rho A \sin^2(n\pi x/l) dx$ which means modal mass, and l is the length of the belt span.

In order to know the nature of the boundary condition at the belt-pulley junction of the axially moving belt, the natural frequencies were measured at the center of the belt span by using the laser velocimetry (B&K 3544). Figure 8 shows the relationship between the first natural frequency and the involved physical parameters: belt thickness and tension. Each data point at a motor speed in Figure 8 was obtained with averaging 3–5 measurements. Young's modulus of the rubber belt was 8×10^9 – $5 \times 10^{10} \text{ N/m}^2$ and much smaller than that of the steel belt/band, i.e., $20 \times 10^{10} \text{ N/m}^2$. The rubber belt is like a string with a negligible

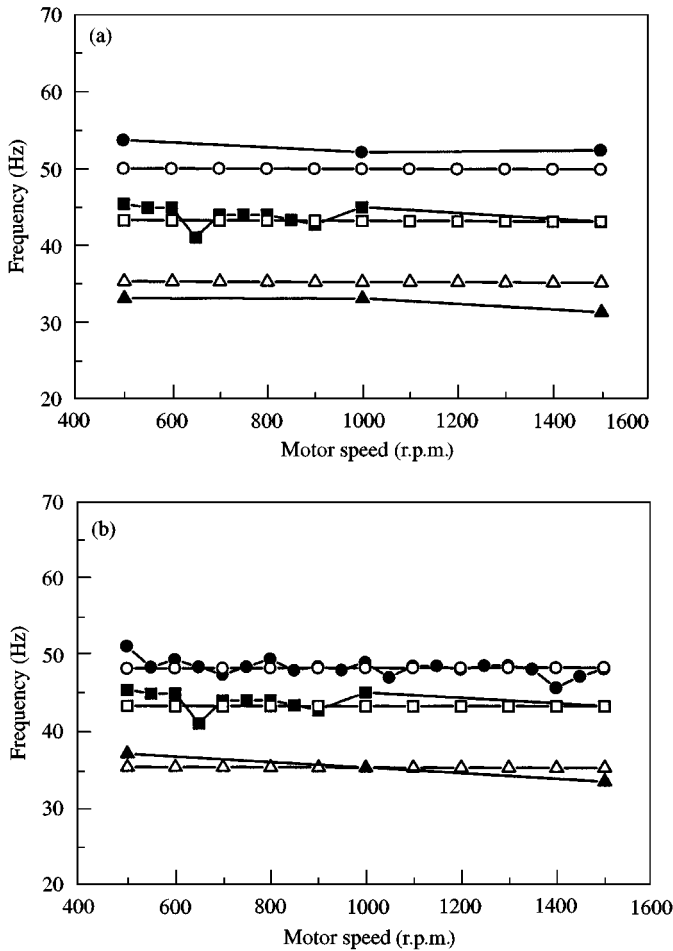


Figure 8. Variation of the fundamental natural frequency of the moving belt due to the change of involved parameters and motor speed. Solid marks denote the measured data and blank marks denote the analytical data. (a) Effect of belt thickness: \circ —, \bullet —, $h = 1.1$ mm; \square —, \blacksquare —, $h = 1.4$ mm; \triangle —, \blacktriangle —, $h = 2.1$ mm. (b) Effect of axial tension: \circ —, \bullet —, $R_0 = 98.0$ N; \square —, \blacksquare —, $R_0 = 73.5$ N; \triangle —, \blacktriangle —, $R_0 = 49.0$ N.

degree of bending stiffness, of which the mass per unit length depends on the belt thickness. Consequently, the natural frequency of the belt decreases as the belt thickness increases. The natural frequency of the belt increases with the increase in belt tension. Although there is a decreasing tendency in natural frequency with increasing speed, its rate is not pronounced. This can be explained by using the ratio of the belt speed to the phase speed of involved bending wave. During the test, the speed range of the belt was 2.62–7.85 m/s that corresponds with the motor speed range of 500–1500 r.p.m. Minimum and maximum values of the motor speed should be compared with the corresponding phase velocity of bending waves. When the phase velocity of bending wave c_{cr} was 89 m/s, the ratios of minimum and maximum belt speed to phase velocity, c_{min}/c_{cr} and c_{max}/c_{cr} , were 0.02 and 0.08 respectively. This explains why the contribution from belt velocity to natural

frequency is small. One can find that the theoretical model assuming the simply supported boundary condition predicts the first natural frequency very closely with motor speed variation. From this reason, the simply supported boundary condition will be used throughout this paper for describing the belt-pulley junctions.

The main cause of transverse vibration of the belt span is usually the excitation due to imperfections in the stiffness of the belt connection. This connection excites the belt periodically at the points where it enters and exits from the free span attached to the pulley bearing surface. When the belt rotates over the drive pulley at a rotational angular velocity ω_p , the point excitation at $x = 0$ can be expressed as

$$w(0, t) = w_0 \exp(jq\omega_p t), \quad (32)$$

where w_0 is the strength of excitation and q is the number of events at which the belt connection enters the free span per rotation. In the theoretical model of the belt vibration, equation (32) should be used as a boundary condition with other simply supported boundary conditions. Figure 9 shows the measurement layout for belt displacement by using a laser velocity sensor at the junction point between free belt span and pulley bearing surface. The length of the connection was 30 mm, the rotating speed was 1000 r.p.m. (or 16.67 Hz), and the belt connection excitation repeated every 0.251 s (or 3.94 Hz). Figure 10(a) shows the measured displacement spectrum, where the first peak is at 3.94 Hz and other major peaks appear at integral multiples of this frequency. A simplified theoretical model is needed for calculating the power flow and this can be done by the truncated spectrum modelling as

$$w(\omega; 0, t) = \sum_{i=1}^n A_i \exp(j\omega_i t), \quad (33)$$

where n is the number of truncated peaks. The coefficients A_i may be obtained from either the slope or the magnitude of the spectrum. The slope can be determined by

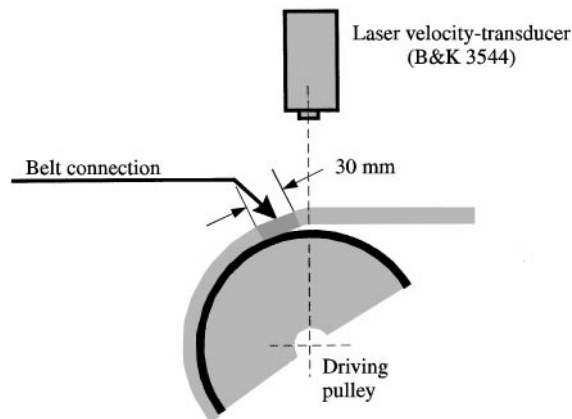


Figure 9. Measurement of the input displacement of the moving belt.

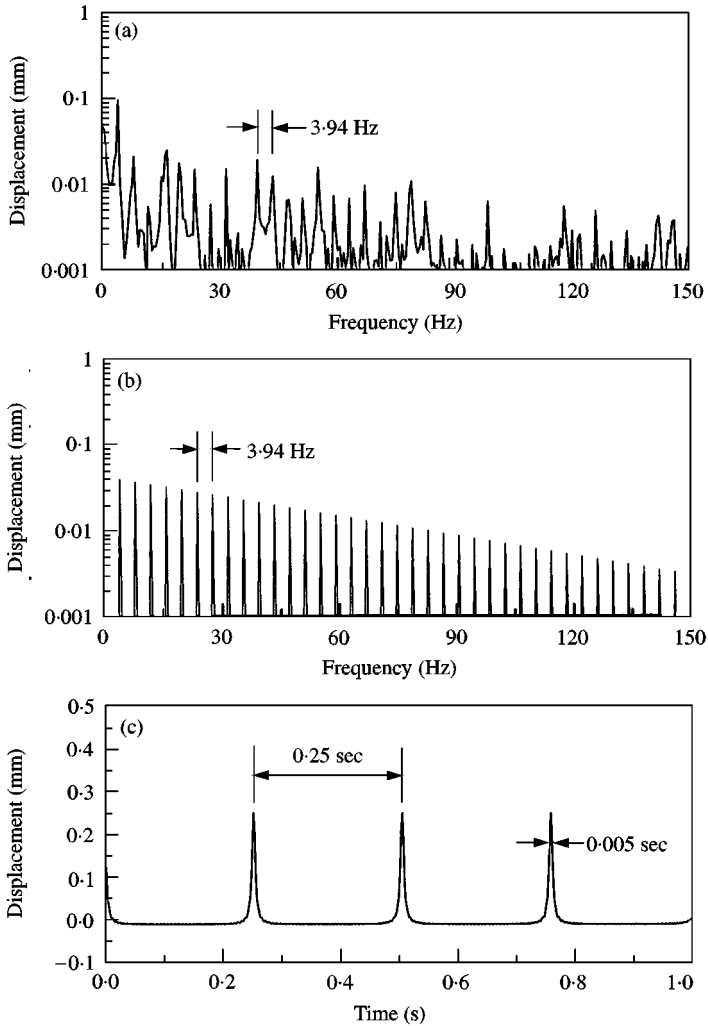


Figure 10. Displacement of the belt connection at 1000 r.p.m.: (a) measured spectra; (b) analytical model in the frequency domain; (c) analytical model in the time domain.

a linear regression of the first to the 38th peak values; the overall magnitude can be determined by the measured overall level. Substitution of proper values into A_i and ω_i in equation (33) yielded Figure 10(b) and the time data in Figure 10(c) was obtained from the inverse Fourier transform of equation (33). One can observe that Figure 10(c) represents the excitation mechanism of the belt-pulley system very well: the peak interval is the same with the rotation cycle of the belt, and the shape of the force function looks impulsive. The time duration passing the length of the connection was 0.005 s at 1000 r.p.m. and, compared with Figure 10(c), the actual time interval was slightly longer than the calculated time. This means that excitation began before the belt connection entered the free span, and ended after the belt connection excited the free span.

There is no power flow in the actual single-span belt-pulley system, because the same amount of the excitation strength is given at each boundary and all powers are totally reflected. However, the power flow can be calculated for this semi-infinite condition if only one pulley is considered and the other part of the belt is considered the only source of the excitation. The calculated results can provide the basic information on the power flow in the moving belt system. Using equation (28b), the spectrum of the true transverse vibrational power flow can be calculated by changing the belt thickness and the modulus of elasticity as shown in Figure 11.

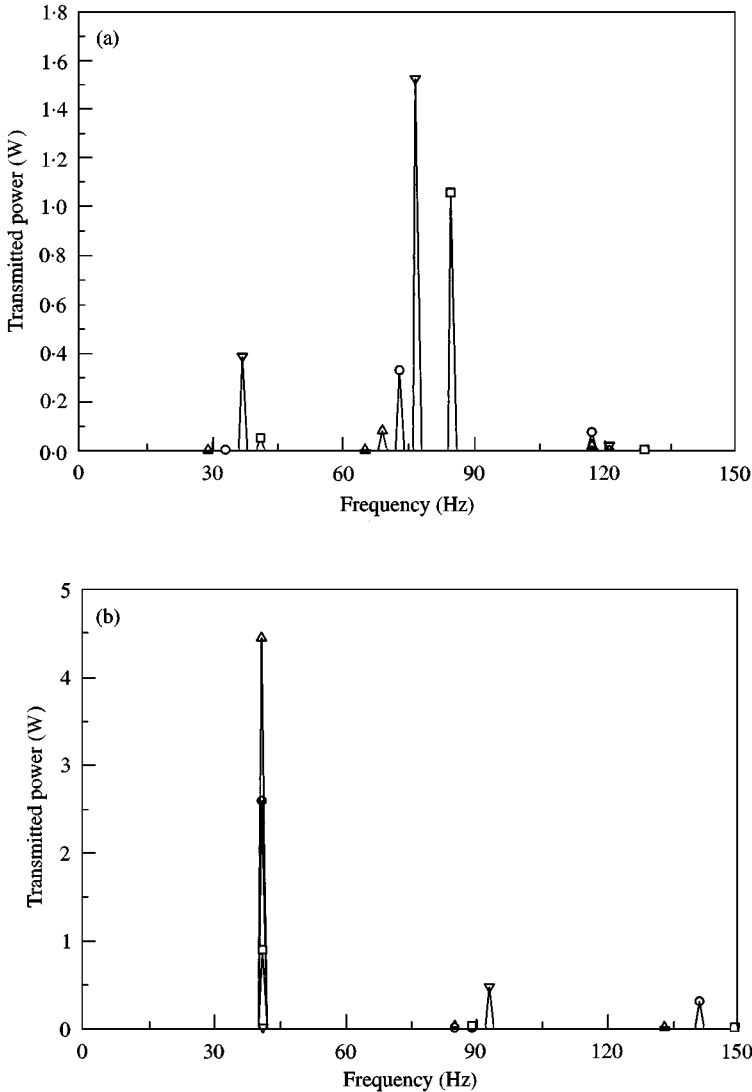


Figure 11. Variation of the vibrational power transmission through the axially moving belt by changing involved parameters. (a) Effect of thickness: \triangle , $h = 2.0$ mm; \circ , $h = 2.5$ mm; \square , $h = 3.0$ mm; ∇ , $h = 4.0$ mm. (b) Effect of Young's modulus: \triangle , $E = 3.0 \times 10^9$ N/m²; \circ , $E = 6.0 \times 10^9$ N/m²; \square , $E = 9.0 \times 10^9$ N/m²; ∇ , $E = 1.2 \times 10^{10}$ N/m².

Transmitted power increases with the increase of thickness, owing to the increase in area moment. It can be seen that the power flow decreases as the modulus of elasticity of the belt increases.

2.4. MULTI-SPAN BELT

2.4.1. *Idler condition*

The multi-span belt–pulley system can be classified into the two conditions according to the involved components: the idler with fixed bearing and the tensioner with a helical spring and a damping mechanism. The physical condition of the single-span belt–pulley system or the simple belt–pulley system with an idler is called the *idler condition*. In this condition, the incident transverse power is assumed to be totally reflected from the points of intersection of belt and pulleys. This is due to the simply supported boundary condition assumed in the foregoing section. No actual power flow exists in the idler condition, so that the observed power flow can be ascribed to that associated with the belt movement only. Therefore, the true power flow can be estimated by using equation (28b) when the idler is replaced by a tensioner. Although the system may possess three or more spans, the transverse vibrational power flow between the first and second spans only will be considered here.

The idler condition can be further categorized into the two conditions. First, the two spans can be coupled at the center hinge between their endpoints. This condition can be adopted in modelling the strong coupling systems such as the steel belt [7]. However, only hard rubber belts are concerned in this study, of which the corresponding coupling between two spans can be considered a weak one. This is because the vibration power transferred from the first span to the second one is very weak in comparison with the input power injected into the second span. When the ends of each span excite adjacent spans as shown in Figure 12, the boundary conditions are given by

$$w_1(0, t) = w_0 \exp(jq\omega_p t), \quad \left. \frac{\partial^2 w_1}{\partial x^2} \right|_{x_1=0} = 0, \quad \left. \frac{\partial^2 w_1}{\partial x^2} \right|_{x_1=l_1} = 0, \quad w_1(l_1, t) = 0, \quad (34-37)$$

$$w_2(0, t) = 0, \quad \left. \frac{\partial^2 w_2}{\partial x^2} \right|_{x_2=0} = 0, \quad \left. \frac{\partial^2 w_2}{\partial x^2} \right|_{x_2=l_2} = 0, \quad w_2(l_2, t) = w_0 \exp(jq\omega_p t). \quad (38-41)$$

Equations (34) and (41) represent excitations at the ends in $x_1 = 0$ and $x_2 = l_2$, respectively, while the simply supported boundary conditions at the ends are shown in equations (35)–(40). Substituting the solution into equations (34)–(41) and equation (11), the vibrational power flow through the axially moving belt can be obtained from equation (19).

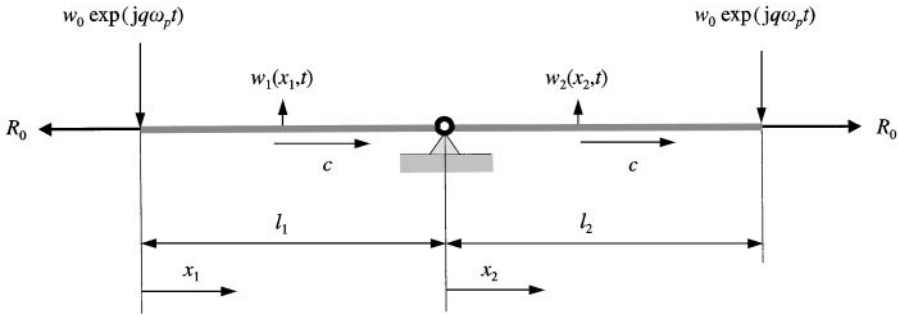


Figure 12. Schematic diagram of the two-belt span modelled as axially moving beams passing through an idler.

2.4.2. Tensioner condition

The reduction of the vibrational power flow through belt–pulley systems is of interest in many practical fields because of the concomitant vibration and noise problems in pulleys, tensioners, and their structural support systems. The tensioner sustaining the appropriate tension in the belt–pulley system also transfers the vibration power. The physical condition of the belt–pulley system with a tensioner as depicted in Figure 13(a) will be called the *tensioner condition*. In Figure 13(b), a schematic diagram is illustrated for the theoretical modelling of vibration power transmission in the belt–pulley system with a tensioner. The boundary conditions specified for the tensioner are as follows:

$$w_1(0, t) = w_0(jq\omega_p t), \quad \left. \frac{\partial^2 w_1}{\partial x^2} \right|_{x_1=0} = 0, \quad w_1(l_1, t) = w_2(0, t), \quad (42-44)$$

$$\left. \frac{\partial^2 w_1}{\partial x^2} \right|_{x_1=l_1} = 0, \quad \left. \frac{\partial^2 w_2}{\partial x^2} \right|_{x_2=0} = 0, \quad (45, 46)$$

$$EI \left. \frac{\partial^3 w_1}{\partial x^3} \right|_{x_1=l_1} - EI \left. \frac{\partial^3 w_2}{\partial x^3} \right|_{x_2=0} = m \left. \frac{\partial^2 w_1}{\partial t^2} \right|_{x_1=l_1} + c_2 \left. \frac{\partial w_1}{\partial t} \right|_{x_1=l_1} + k_{s2} w_1(l_1, t), \quad (47)$$

$$\left. \frac{\partial^2 w_2}{\partial x^2} \right|_{x_2=l_2} = 0, \quad w_2(l_2, t) = w_0(jq\omega_p t). \quad (48, 49)$$

The displacement of the tensioner as a common support of the two-belt spans at $x_1 = l_1$ (or $x_2 = 0$) should be the same for both spans in equation (44). In equations (45) and (46), the moment is zero at the common support and the simple mass, damper, spring system in equation (47) describes the tensioner dynamics for balancing the shear force. The same procedure as the preceding section should be followed for estimating the vibrational power flow through the moving belt.

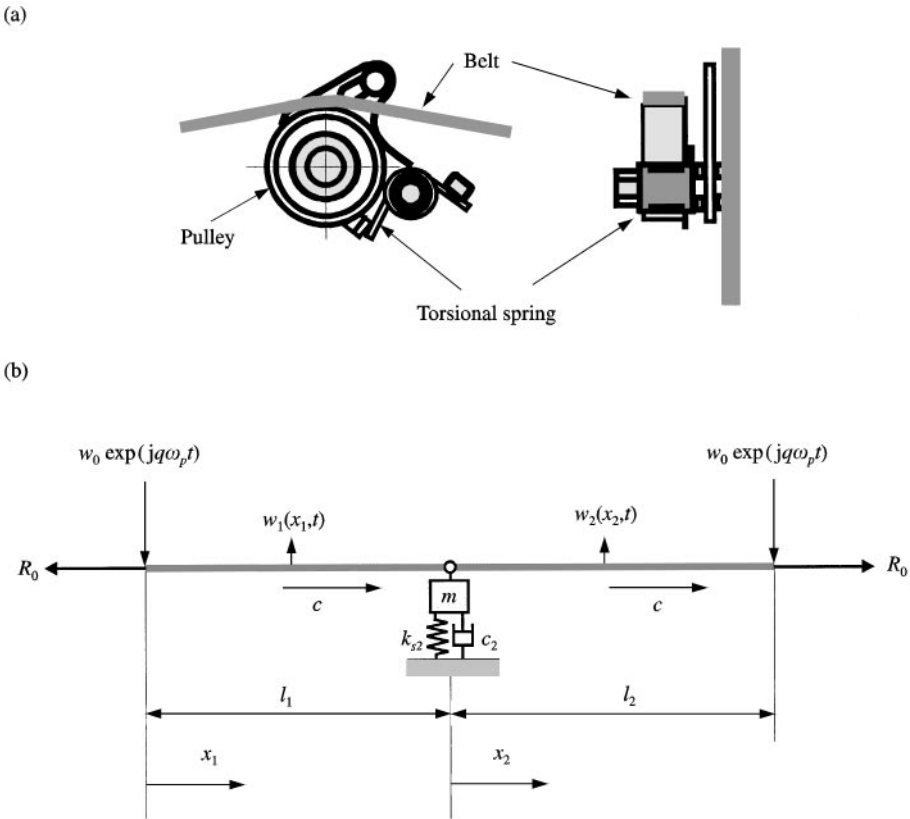


Figure 13. (a) Configuration of the typical belt tensioner, (b) schematic diagram of the two-belt span modelled as axially moving beams passing through a tensioner.

3. COMPARISON OF THEORETICAL AND EXPERIMENTAL RESULTS

3.1. MEASUREMENT METHOD

Based on the finite difference approximation, the vibrational power flow can be determined from the cross-spectral density measured by two closely spaced laser velocity sensors as follows [24]:

$$\Pi = \frac{2\sqrt{\rho AEI}}{\Delta} \text{Im}(G_{21}). \tag{50}$$

Here, $G_{21}(\omega)$ is the one-sided cross-spectral density between the two measured velocities at points 1 and 2, and Δ is the laser-beam spacing. Phase difference between channels was compensated for precise measurement. The experimental set-up was as shown in Figure 14. The test system consisted of two driving and driven pulleys of 100 mm in diameter and the separation between the two shafts was 500 mm. The distance between the shafts of the drive pulley and the idler or tensioner was 0.2 m in the x direction. The distance between the shafts of the driven pulley and the idler or tensioner was 0.3 m in the x direction. A speed-controllable

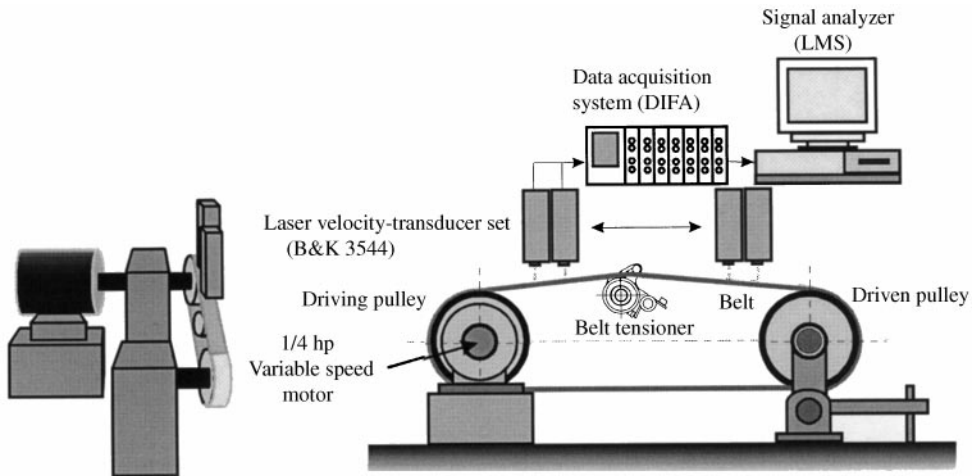


Figure 14. Configuration of the two-span belt-pulley system and the measurement set-up for measuring the energy flow in axially moving belt including a tensioner.

1/4-hp motor drove the driving pulley and the rotation speed was adjustable from 500 to 1500 r.p.m., while the driven pulley was unloaded. The rectangular cross-section of the rubber belt was $2.1 \text{ mm} \times 20 \text{ mm}$ and the belt tension was 98 N. A pair of laser sensors separated by 0.02 m measured the power flow at the center of each span in a non-contact manner.

3.2. IDLER CONDITION

In Figure 15, the calculated power flow in the first and second spans are compared with the measured ones for the idler condition at 1000 r.p.m. It is noted that most of the vibrational energy flows are concentrated in the region of the first natural frequency of the belt. Under this idler condition, because the damping mechanism of the support structure does not exist, the power flow in Figures 15(a) and (b) is associated only with the internal damping of the belt and the effect of medium motion. The negative power flow for the first span means that the effect of medium movement is dominant compared with the contribution from internal damping. In contrast, the magnitude of the second span as shown in Figures 15(c) and (d) is smaller than that of the first span. This is because the direction of power flow caused by both the internal damping of the belt and the effect of medium motion is nearly the same. The direction of vibration power flow is opposite to that of the belt movement. It is observed that there is a reasonable degree of agreement between calculated and measured data, although small differences between magnitudes occur. This discrepancy arises from the fact that each span of the actual system was excited at two end positions while each span of the theoretical model was excited by only one end.

3.3. TENSIONER CONDITION

Comparison between measured and calculated data is shown in Figure 16 for the tensioner condition at 1000 r.p.m. In Figures 16(a) and (b), measured and

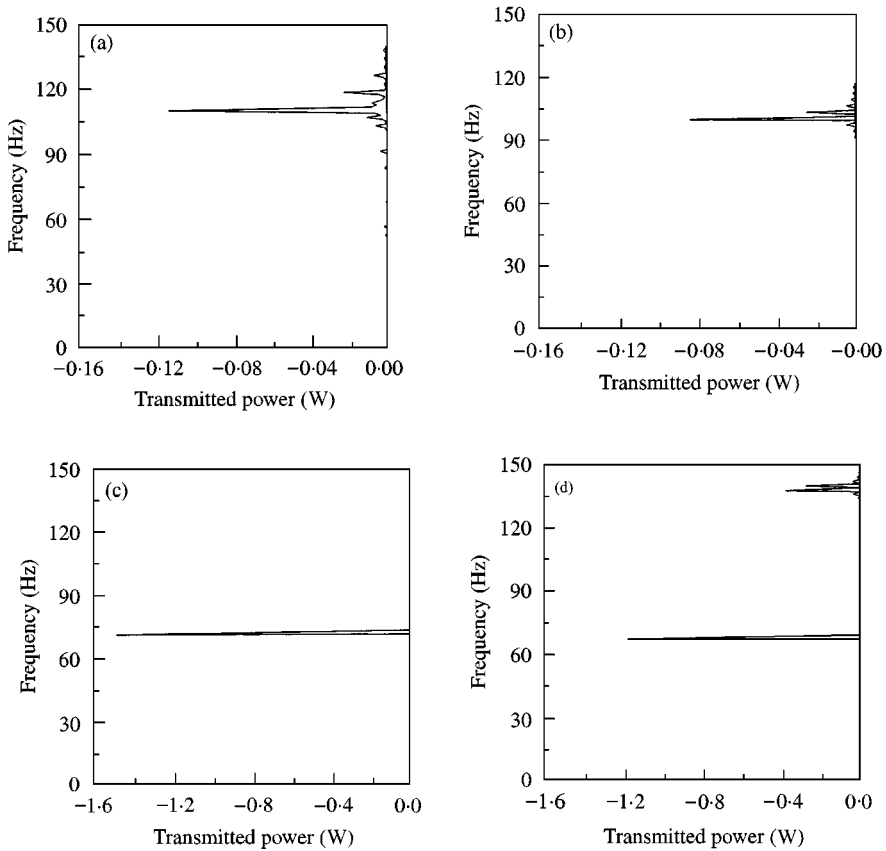


Figure 15. Vibrational power flow in the belts passing through an idler at 1000 r.p.m. (a), (b) Measured and calculated data at the first span; (c), (d) measured and calculated data at the second span.

calculated power flows through the first span were -0.002 and -0.020 W respectively. Under this tensioned condition, the damping mechanism of support structure can exist. Consequently, the power flow in Figures 16(a) and (b) includes all effects from the internal damping of the belt, the damping mechanism of support structure, and the medium movement. The negative power flow for the first span means that the effect of belt movement is again dominant compared with the internal damping of the belt and the damping mechanism of the support structure. Resultant magnitudes are larger than those of the idler condition because the true power component was added in this case. The two conditions in Figures 15 and 16 are compared for the first span and their differences in measurement and calculation were 0.094 and 0.06 W respectively. The difference is due to the damping mechanism within the tensioner. Measured and calculated power flows through the second span are shown in Figures 16(c) and (d). The magnitude of power flow in the second span is smaller than that of the first span. This is because the direction of power flow is identical for three involved mechanisms, i.e., the internal damping of belt, the effect of medium motion, and the damping mechanism

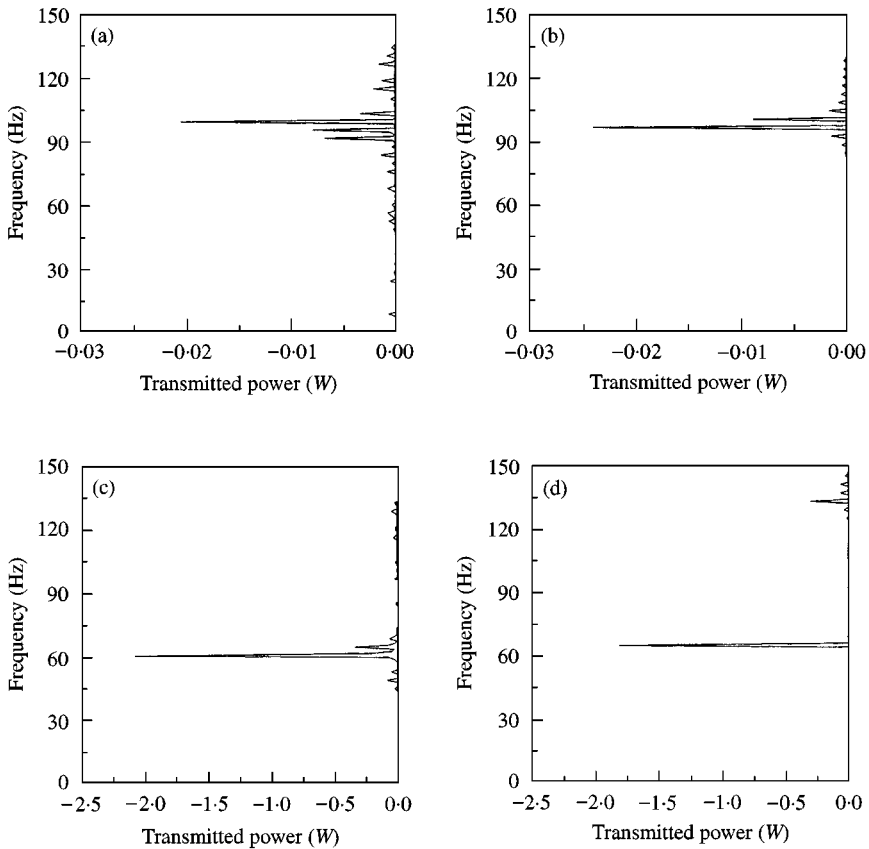


Figure 16. Vibrational power flow in the belts passing through a tensioner at 1000 r.p.m. (a), (b) Measured and calculated data at the first span; (c), (d) measured and calculated data at the second span.

of support structure. Measured and calculated transverse power flows were -2.1 and -1.8 W respectively. Differences in the measured and the calculated magnitudes between the two conditions in Figures 15 and 16 were -0.6 and -0.62 W respectively. When equation (28b) is employed, the true power flow through the moving belt can be obtained. Figure 17 shows the measured and calculated true power flow through two spans. The difference is caused by the small difference in boundary conditions between the actual system and the calculation model. In Figure 17(a), the direction of power flow through the first span is positive, i.e., from the driving pulley to the tensioner. In Figure 17(b), the direction of power flow through the second span is negative, i.e., from the driven pulley to the tensioner. These results clearly show that the vibration power is transmitted from the belt-pulley junctions to the tensioner.

3.4. PARAMETRIC STUDY

By using the proposed method, the characteristics of vibration power of the tensioner can be predicted by changing the involved dynamic parameters of belt

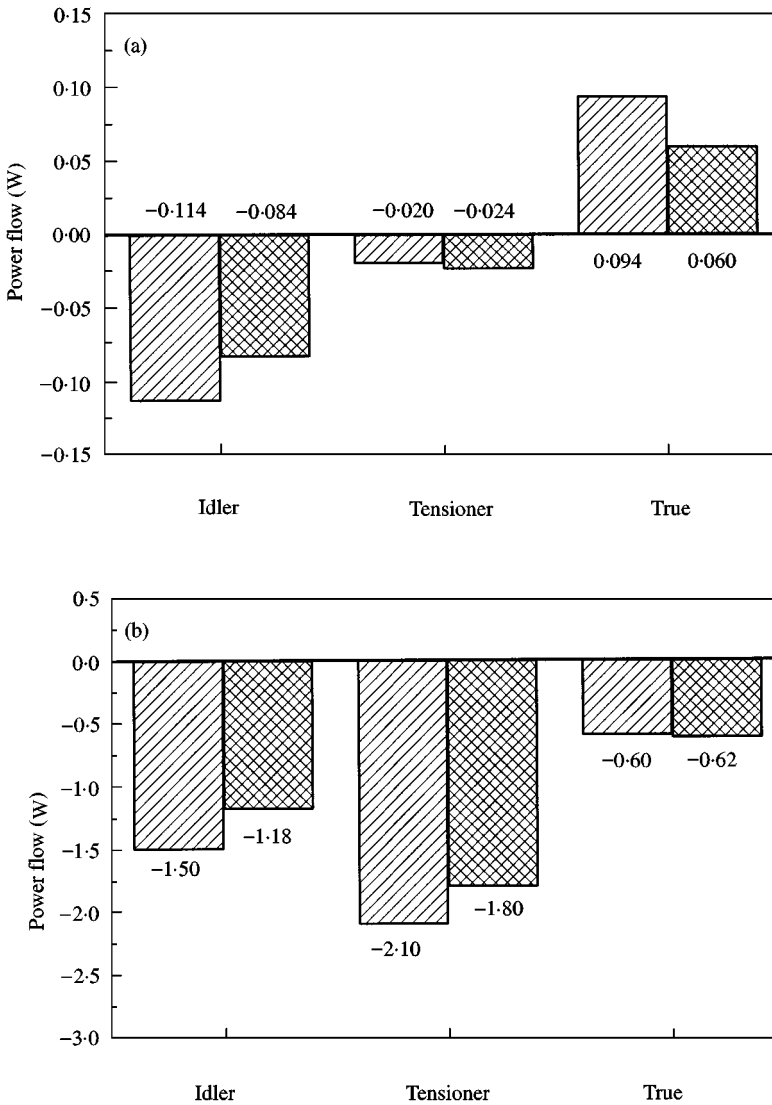
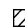

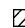



Figure 17. Actual vibrational power flow through two-belt spans. (a) First span: , measured; , calculated. (b) Second span: , measured; , calculated.

and tensioner. In Figure 18(a), one can find that the vibrational energy flow increases as the belt thickness increases. Figure 18(b) shows the decreasing trend of power flow with the increase of loss factor of the belt. As the spring constant of the tensioner increases, the tensioner becomes more difficult to move and the power flow from the belt decreases as seen in Figure 18(c).

4. CONCLUSION

In this study, vibrational power transmission in axially moving belts with pulleys and tensioners was studied analytically and experimentally. It was shown that the

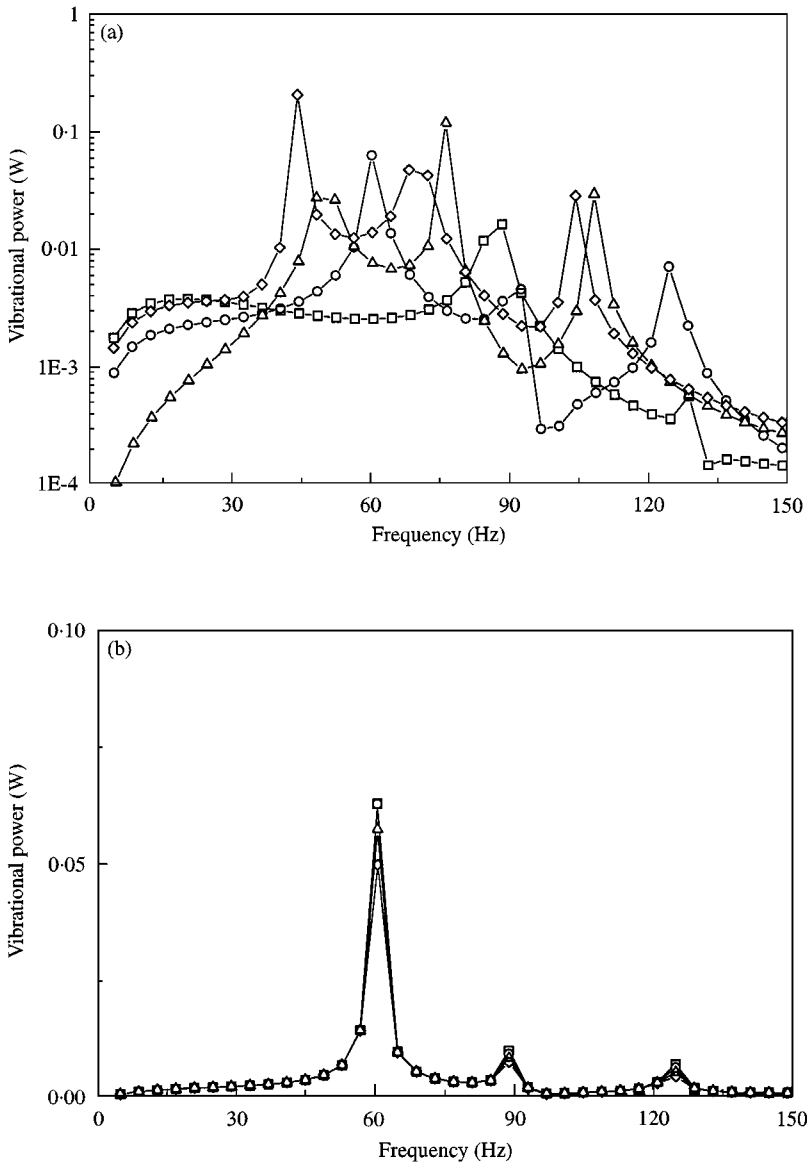


Figure 18. Change of the transmitted vibrational power to the tensioner by varying the physical parameters. (a) Belt thickness: \square , $h = 1$ mm; \circ , $h = 2$ mm; \triangle , $h = 3$ mm; \diamond , $h = 4$ mm. (b) Loss factor of the belt: \square , $\eta = 0.05$; \circ , $\eta = 0.10$; \triangle , $\eta = 0.15$; \diamond , $\eta = 0.20$. (c) Spring constant of the tensioner: \square , $k_{s2} = 1e4$ N/m; \circ , $k_{s2} = 1e5$ N/m; \triangle , $k_{s2} = 1e6$ N/m.

total vibrational power flow is the sum of the true power flow and the power component associated with the belt movement. By utilizing the fact that the wave is totally reflected in the idler condition, the net power flow into the tensioner could be obtained. It was shown that the direction of the vibrational power flow from both belt spans is pointing toward the tensioner. Results of the parametric study

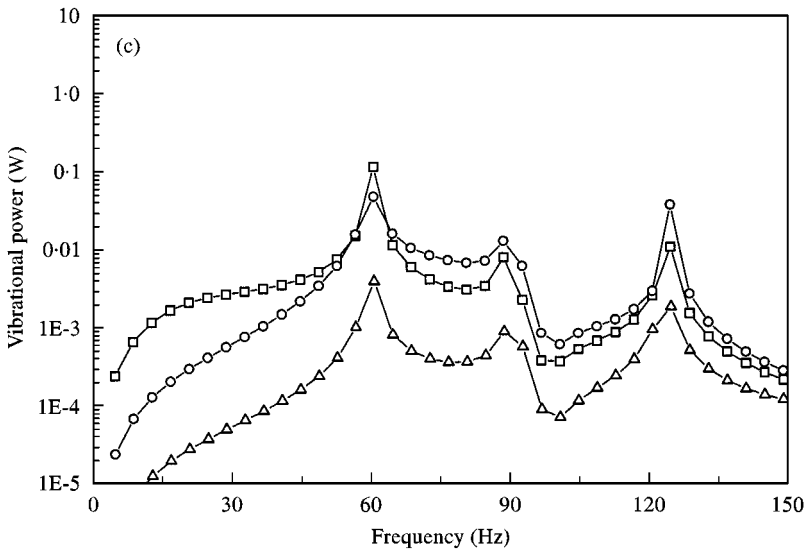


Figure 18. Continued.

showed that the power flow into the tensioner decreases with the decrease of belt thickness or the increase of loss factor and/or stiffness of the tensioner. It is thought that the analytical method proposed in this paper provides a clue for solving the vibration and noise problems in association with the belt-pulley systems.

However, only the idler condition with weak coupling is dealt with in this paper. The strongly coupled belts should be further investigated in order to account for the energy transmission over the idler that can be observed in metallic belts. In the latter case, it is thought that quite precise consideration should be given to the wave reflection from the belt-pulley or belt-idler junction. Even the weakly coupled belts such as the rubber belts, the wave reflection coefficient of the belt-pulley junction should be carefully measured for more precise quantitative evaluation of the power flow. One may extend the theory by including other types of excitation such as the pulley vibrations of torsional, bending or their combinations. The study of the belt-induced noise and vibration would be fruitful if the effect of the structural mobility of the supporting structure for pulley shafts and tensioners is investigated further.

REFERENCES

1. T. KOYAMA, K. WATANABE, K. NAGAI and M. KAGOTANI 1990 *Transactions of the American Society of Mechanical Engineers, Journal of Mechanical Design* **112**, 419-429. A study on timing belt noise.
2. C. D. MOTE JR 1965 *Journal of the Franklin Institute* **279**, 430-444. A study of band saw vibrations.
3. C. D. MOTE JR and S. NAGULESWARAN 1966 *Transactions of the American Society of Mechanical Engineers, Journal of Engineering for Industry* **88**, 151-156. Theoretical and experimental band saw vibrations.

4. J. A. WICKERT and C. D. MOTE JR 1988 *Shock and Vibration Digest* **20**, 3–13. Current research on the vibration and stability of axially-moving materials.
5. J. A. WICKERT and C. D. MOTE JR 1990 *Transactions of the American Society of Mechanical Engineers, Journal of Applied Mechanics* **57**, 738–744. Classical vibration analysis of axially moving continua.
6. J. MOON and J. A. WICKERT 1997 *Journal of Sound and Vibration* **200**, 419–431. Non-linear vibration of power transmission belts.
7. A. G. ULSOY 1986 *Transactions of the American Society of Mechanical Engineers, Journal of Vibration, Acoustics, Stress, and Reliability in Design* **108**, 207–212. Coupling between spans in the vibration of axially moving materials.
8. A. A. N. AL-JAWI, C. PIERRE and A. G. ULSOY 1995 *Journal of Sound and Vibration* **179**, 243–266. Vibration localization in dual-span, axially moving beams, Part I: formulation and results.
9. A. A. N. AL-JAWI, C. PIERRE and A. G. ULSOY 1995 *Journal of Sound and Vibration* **179**, 267–287. Vibration localization in dual-span, axially moving beams, Part II: perturbation analysis.
10. A. A. N. AL-JAWI, A. G. ULSOY and C. PIERRE 1995 *Journal of Sound and Vibration* **179**, 289–312. Vibration localization in band-wheel systems: theory and experiment.
11. C. D. MOTE JR and W. Z. WU 1985 *Journal of Sound and Vibration* **102**, 1–9. Vibration coupling in continuous belt and band systems.
12. K. W. WANG and C. D. MOTE JR 1986 *Journal of Sound and Vibration* **109**, 237–258. Vibration coupling analysis of band/wheel mechanical systems.
13. A. G. ULSOY, J. E. WHITESSELL and M. D. HOOVEN 1985 *Transactions of the American Society of Mechanical Engineers, Journal of Vibration, Acoustics, Stress, and Reliability in Design* **107**, 282–290. Design of belt-tensioner systems for dynamic stability.
14. A. A. RENSHAW, C. D. RAHN, J. A. WICKERT and C. D. MOTE 1998 *Transactions of the American Society of Mechanical Engineers, Journal of Vibration and Acoustics* **120**, 634–636. Energy and conserved functionals for axially moving material.
15. J. A. WICKERT and C. D. MOTE JR 1989 *The Journal of the Acoustical Society of America* **85**, 1365–1368. On the energetic of axially-moving continua.
16. G. PAVIC 1976 *Journal of Sound and Vibration* **49**, 221–230. Measurement of structure borne wave intensity, Part I: formulation of the methods.
17. C. J. WU and R. G. WHITE 1995 *Journal of Sound and Vibration* **181**, 99–114. Vibrational power transmission in a finite multi-supported beam.
18. C. J. WU and R. G. WHITE 1995 *Journal of Sound and Vibration* **187**, 329–338. Reduction of vibrational power in periodically supported beams by use of a neutralizer.
19. S. NAGULESWARAN and C. J. H. WILLIAMS 1968 *International Journal of the Mechanical Sciences* **10**, 239–250. Lateral vibration of band-saw blades, pulley belts and the like.
20. W. T. RIM and K. J. KIM 1994 *Mechanical Systems and Signal Processing* **8**, 199–213. Identification of tension in a belt-driven system by analyzing flexural vibration.
21. K. W. WANG and C. D. MOTE JR 1987 *Journal of Sound and Vibration* **115**, 203–216. Band/wheel system vibration under impulsive boundary excitation.
22. W. T. RIM 1993 *Ph.D. thesis, Department of Mechanical Engineering, Korea Advanced Institute of Science and Technology, Taejon, Korea*. Identification of static and dynamic tension in belt driving systems using flexural vibration.
23. H. G. GOYDER and R. G. WHITE 1980 *Journal of Sound and Vibration* **68**, 59–75. Vibrational power from machines into built-up structure, Part I: introduction and approximate analysis of beam and plate-like foundations.
24. J. W. VERHEIJ 1980 *Journal of Sound and Vibration* **70**, 133–139. Cross-spectral density methods for measuring structure borne power flow on beams and pipes.